Advanced Robotics, Vol. 10, No. 1, pp. 81–103 (1996)

Paper

Optimal grid pattern for focal length calibration

KENICHI KANATANI and TAMOTSU MARUYAMA*

Department of Computer Science, Gunma University, Kiryu 376, Japan
**ALTRON Co., 5-9-41 Kitashinagawa, Shinagawa-ku, Tokyo 141, Japan*

Received 16 February 1994; accepted 22 August 1995

Abstract—An optimal grid pattern is designed so that the reliability of the camera focal length calibration using it is theoretically maximized. The analysis is based on a statistical error model of line fitting in digital images. The reliability of the focal length is quantitatively computed from the reliability of the vanishing points and the reliability of the vanishing points is quantitatively computed from the reliability of the edges to which lines are fitted. A realistic device is designed by adding many technical improvements and a prototype model is shown.

1. INTRODUCTION

Visual sensing plays a central role in controlling robots that recognize environments and computing three-dimensional (3D) structures from images requires the imaging geometry of the camera. Hence, the camera model must be adjusted so that it agrees with the actual camera. This process is called *camera calibration* and is now one of the most important problems in robotics applications [1–10]. From among many parameters, this paper specifically deals with the *focal length*. This is because the focal length plays the most fundamental role in bridging 3D and 2D geometries. However, other parameters are also important.

For example, straight lines may not be projected to straight lines due to optical distortion of the lens (*aberration*), so an appropriate mapping (*geometric correction*) must be applied for removing it. Another important parameter is the *aspect ratio* — the ratio of the horizontal scale to the vertical scale. The *image origin* must also be located accurately. In the past, many researchers have tried to estimate all the parameters in one stage. A typical procedure is follows:

(1) Set, in the scene, multiple reference markers (points, lines, squares, circles, etc.) whose 3D locations and shapes are known.

(2) Construct a parameterized camera model that incorporates all factors, and describe the predicted 2D locations and shapes of the reference markers in terms of the model parameters.

(3) Adjust the model parameters by minimizing the discrepancy between the predicted description and the actually obtained description of the reference markers.

However, many problems arise in this approach. For example, the function to be minimized is usually highly non-linear in the model parameters, so numerical iterations are necessary, but global convergence is not guaranteed in general: the search may be trapped into a local minimum. If lens and image distortions are neglected, the equations can be 'linearized' by introducing auxiliary variables ('homogeneous coordinates'), and in appearance the optimization reduces to solving simultaneous linear equations. However, what is actually minimized is not clear if such artificial linearization is involved.

Even if the parameter values that attain the minimum are found, this does not necessarily mean that each value is reliable, because one parameter may be greatly perturbed to compensate for errors in other parameters. This typically occurs when parameters of different geometric origins are mixed. For example, in order to estimate the local length accurately, the effect of foreshortening must be strong: assuming different focal lengths does not affect the resulting 3D interpretation very much unless foreshortening is apparent. Hence, if a planar pattern is used, it must be placed so that it makes a large angle with the image plane, whereas if the 3D camera position is to be computed by using the same pattern, a reliable estimate is obtained when it is placed nearly parallel to the image plane. In other words, the mechanism of estimation is different from parameter to parameter, each requiring a different and sometimes conflicting condition for high accuracy.

Thus, the calibration procedure should be decomposed into separate modules corresponding to individual parameters. Then, each module should be designed so that *its reliability is maximized* and the reliability of the resulting estimate must be evaluated *in quantitative terms*. With this motivation, Kanatani [11] presented a rigorous mathematical theory for quantitatively evaluating the reliability of focal length calibration by using a rectangular grid pattern and computed the configuration that has maximum reliability.

In this paper, we attain *higher* reliability than the theoretical bound presented in [11]. This is made possible by using a *non-rectangular* grid pattern. Applying the theory presented in [11], we design the grid pattern so that the theoretically predicted reliability is maximized. Following [11], we also compute the confidence interval for the computed focal length. Finally, a prototype model is designed by incorporating many realistic improvements.

2. PERSPECTIVE PROJECTION AND N-VECTORS

We assume the camera model shown in Fig. 1 [12–14]; we call the origin O the *viewpoint* and the constant f the *focal length*. A point on the image plane is represented by a unit vector $\boldsymbol{m}$, which indicates the orientation of the ray that starts from the viewpoint O and passes through that point; a line on the image plane is represented by the unit surface normal $\boldsymbol{n}$ to the plane that passes through the viewpoint O and

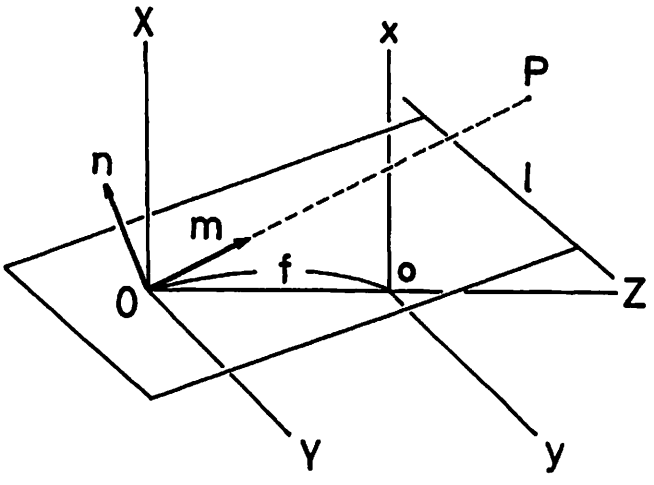

Figure 1. Imaging geometry and N-vectors of a point and a line.

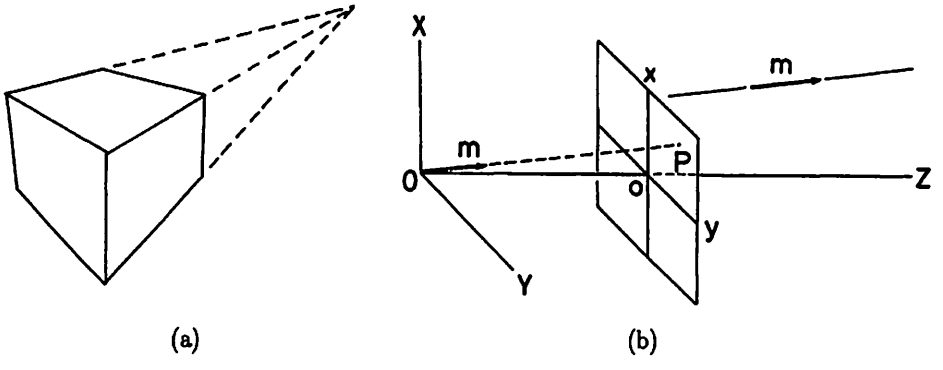

Figure 2. (a) Vanishing point. (b) The N-vector of the vanishing point of a space line.

intersects the image plane along that line (Fig. 1). We call $\boldsymbol{m}$ and $\boldsymbol{n}$ the *N-vectors* of the point and the line [13, 14].

The N-vector of a point in the scene is defined to be the N-vector of its projection on the image plane and the N-vector of a line in the scene is defined to be the N-vector of its projection on the image plane. In the following, we call a point in the scene a *space point* and a point on the image plane an *image point*. Similarly, a line in the scene is called a *space line*; a line on the image plane is called an *image line*.

As is well known, projections of parallel space lines meet at a common *vanishing point* on the image plane (Fig. 2a). From Fig. 2(b), we observe that a space line that extends along unit vector $\boldsymbol{m}$ has, when projected, a vanishing point of N-vector $\pm\boldsymbol{m}$ [12–14].

3. STATISTICAL MODEL OF LINE FITTING

In conventional image processing, edges are detected by the Hough transform or an edge operator, and a set of edge pixels is obtained by applying thresholding and thinning processes. Then, lines are fitted to the edge pixels by least squares. Since vanishing points are estimated as intersections of fitted lines, the reliability of the vanishing points depends on the reliability of the edges. Thus, we need a statistical model for the error behavior of line fitting to edge pixels.

Let $\bar{\boldsymbol{n}}$ be the N-vector of an image line fitted to edge pixels in the absence of noise. In the presence of noise, each edge pixel is displaced. Let $\boldsymbol{n} = \bar{\boldsymbol{n}} + \Delta\boldsymbol{n}$ be the N-vector of the image line fitted to the displaced edge pixels. Since the noise behavior is random, the error $\Delta\boldsymbol{n}$ is regarded as a random variable. We define the *covariance matrix* of $\boldsymbol{n}$ by

$$V[\boldsymbol{n}] = E[\Delta\boldsymbol{n}\Delta\boldsymbol{n}^{\top}], \tag{1}$$

where $E[\cdot]$ means expectation and $\top$ denotes transpose.

The theoretical expression for this covariance matrix was derived from a statistical model of image noise in [14, 15]. Since the derivation requires a lengthy analysis, we omit the details and show the final form:

$$V[\boldsymbol{n}] \approx \frac{6\kappa}{w^3}\boldsymbol{u}\boldsymbol{u}^{\top} + \frac{\kappa}{2f^2 w}\boldsymbol{m}_G\boldsymbol{m}_G^{\top}. \tag{2}$$

Here, w is the length (measured in pixels) of the edge segment; $\boldsymbol{u}$ is its orientation; $\boldsymbol{m}_G$ is the N-vector of the center point G of the edge segment (Fig. 3). If $\boldsymbol{m}_a$ and $\boldsymbol{m}_b$ are the N-vectors of the end points of the edge segment, the orientation $\boldsymbol{u}$ is formally defined by $\boldsymbol{u} = \pm N[\boldsymbol{m}_a - \boldsymbol{m}_b]$. The constant κ is called the *image resolution* and defined by

$$\kappa = \frac{\varepsilon^2}{\rho}, \tag{3}$$

where ε is the *image accuracy* defined as the root mean square of the displacement of each edge pixel, while ρ is the *edge density* defined as the number of edge pixels

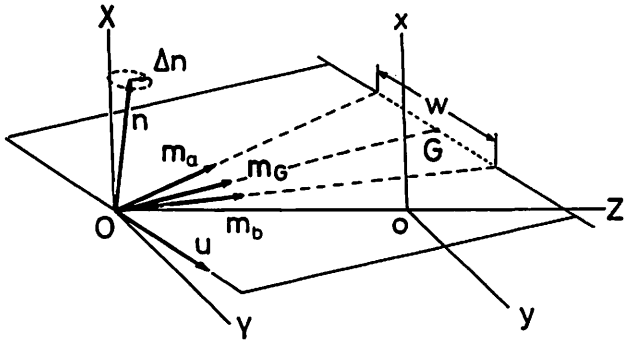

Figure 3. Line fitting to an edge segment.

per unit pixel length. It has been experimentally confirmed that (2) is a very good approximation [14, 15].

4. OPTIMAL ESTIMATION OF VANISHING POINTS

If image lines $\{l_\alpha\}$, $\alpha = 1, \ldots, N$, are projections of parallel space lines, they are *concurrent* on the image plane, meeting at their vanishing point. Let $\{n_\alpha\}$, $\alpha = 1, \ldots, N$, be the N-vectors of concurrent image lines. We see from Fig. 4a that $(m, n_\alpha) = 0$, $\alpha = 1, \ldots, N$ (in this paper, we use $(\cdot, \cdot)$ to denote the inner product of vectors). Hence, the N-vector m of the common intersection is robustly computed by the following least-squares optimization in the presence of noise:

$$\sum_{\alpha=1}^{N} W_\alpha (m, n_\alpha)^2 \to \min . \tag{4}$$

The weights W_α should be determined so that reliable data are given large weights while unreliable data are given small weights. It can be shown that the optimal weights are given as follows [14, 15]:

$$W_\alpha = \frac{1}{(m, V[n_\alpha]m)}. \tag{5}$$

Since

$$\sum_{\alpha=1}^{N} W_\alpha (m, n_\alpha)^2 = (m, \Big(\sum_{\alpha=1}^{N} W_\alpha n_\alpha n_\alpha^\top\Big)m), \tag{6}$$

the solution of the optimization (4) is given by the unit eigenvector of the *moment matrix*

$$N = \sum_{\alpha=1}^{N} W_\alpha n_\alpha n_\alpha^\top \tag{7}$$

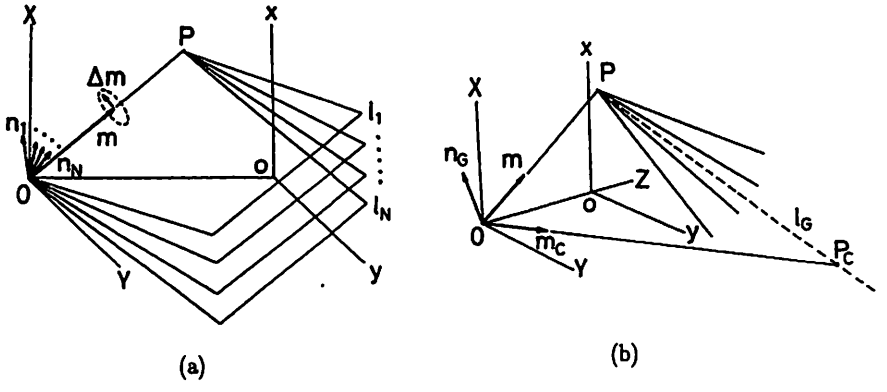

Figure 4. (a) The common intersection of concurrent lines. (b) The center line l_G of concurrent lines. Point P_C is conjugate to the vanishing point P on line l_G.

for the smallest eigenvalue. Note that the optimal weights contain the N-vector $\boldsymbol{m}$ we want to compute. Also, it can be shown that the estimate given by (4) has *statistical bias* [15]. These difficulties can be resolved by a method called *renormalization* [15] (see Appendix).

By applying the *perturbation theorem*, the covariance matrix $V[\boldsymbol{m}]$ of the computed N-vector $\boldsymbol{m}$ of the vanishing point is evaluated in the following form [14, 15]:

$$V[\boldsymbol{m}] = \frac{\boldsymbol{u}\boldsymbol{u}^\top}{\lambda_u} + \frac{\boldsymbol{v}\boldsymbol{v}^\top}{\lambda_v}. \tag{8}$$

Here, λ_u and λ_v are the largest and intermediate eigenvalues of the moment matrix $\boldsymbol{N}$ defined by (7), and $\boldsymbol{u}$ and $\boldsymbol{v}$ are the corresponding unit eigenvectors.

Let $\boldsymbol{n}_G$ be the unit eigenvector of $\boldsymbol{N}$ for the largest eigenvalue. Vector $\boldsymbol{n}_G$ can be regarded as the N-vector of a hypothetical *center line* l_G of the N lines (Fig. 4b). Since the three eigenvectors form an orthonormal system, the unit eigenvector $\boldsymbol{m}_C$ for the second largest eigenvalue equals $\pm\boldsymbol{m} \times \boldsymbol{n}_G$. Vector $\boldsymbol{m}_C$ is orthogonal to both $\boldsymbol{n}_G$ and $\boldsymbol{m}$ and hence can be identified with the N-vector of the point P_C 'conjugate'[13] to the vanishing point P on the center line l_G.

Let ϕ_α be the angle between $\boldsymbol{n}_G$ and $\boldsymbol{n}_\alpha$; we call it the *deviation angle* (from the hypothetical center line). Let θ_α be the angle between $\boldsymbol{m}_{G\alpha}$ and $\boldsymbol{m}$; we call it the *disparity* (of the vanishing point from the center point of the αth edge segment). Let w_α be the length of the αth edge segment. If the covariant matrix $V[\boldsymbol{n}_\alpha]$ of the image line fitted to each edge segment is given in the form of (2), it can be proved that the covariance matrix $V[\boldsymbol{m}]$ given by (8) has the following approximation [11]:

$$V[\boldsymbol{m}] \approx \frac{6\kappa \boldsymbol{m}_C \boldsymbol{m}_C^\top}{\sum_{\alpha=1}^{N} w_\alpha^3 \sin^2\phi_\alpha / \sin^2\theta_\alpha}. \tag{9}$$

5. DETERMINATION OF THE FOCAL LENGTH

When we analyze images in terms of N-vectors, we are modeling the camera imaging geometry as perspective projection (Fig. 1). This model can be *hypothetical*: it need not correspond to the actual camera *as long as no 3D interpretation is involved*. For example, when we compute vanishing points as intersections of concurrent image lines, the camera model can be arbitrarily assumed. However, if we want to infer 3D relationships such as 3D orientations of space lines and surfaces and their orthogonality in the scene, the resulting 3D interpretations are valid only when the camera model exactly agrees with the imaging geometry.

From the definition of the N-vector, it is easily shown that if $\boldsymbol{m} = (m_1, m_2, m_3)^\top$ is the N-vector of an image point defined with respect to focal length f and if $\hat{\boldsymbol{m}} = (\hat{m}_1, \hat{m}_2, \hat{m}_3)^\top$ is the N-vectors of the same image point defined with respect to a different focal length $\hat{f}$, they should satisfy the following relation [11] (Fig. 5a):

$$\hat{\boldsymbol{m}} = \pm N\left[\begin{pmatrix} m_1 \\ m_2 \\ (\hat{f}/f)m_3 \end{pmatrix}\right]. \tag{10}$$

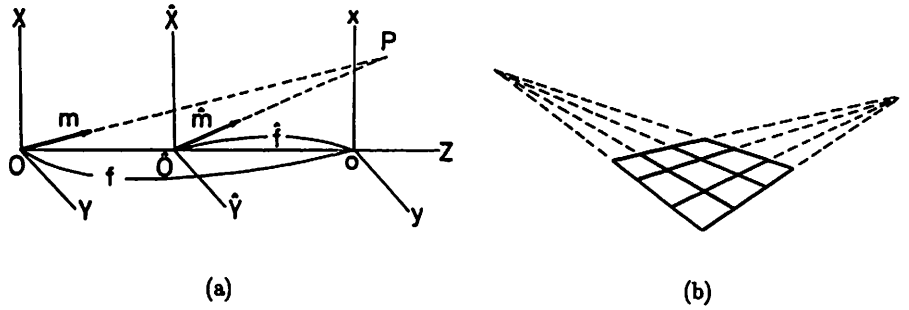

(a) (b)

Figure 5. (a) N-vectors of image points and image lines are altered if the focal length f is altered. (b) Vanishing points of two sets of parallel space lines making a known angle in the scene.

Here, the symbol $N[\cdot]$ denotes normalization into a unit vector.

Let $\boldsymbol{m} = (m_1, m_2, m_3)^\top$ and $\boldsymbol{m}' = (m_1', m_2', m_3')^\top$ be the N-vectors, defined with respect to a tentative focal length f, of the vanishing points of space lines that make a known angle α (Fig. 5b). Since the expressions for $\boldsymbol{m}$ and $\boldsymbol{m}'$ with respect to the true focal length $\hat{f}$ are given in the form of (10), we obtain the following equality:

$$m_1 m_1' + m_2 m_2' + \left(\frac{\hat{f}}{f}\right)^2 m_3 m_3' = \sqrt{m_1^2 + m_2^2 + \left(\frac{\hat{f}}{f}\right)^2 m_3^2}\sqrt{m_1'^2 + m_2'^2 + \left(\frac{\hat{f}}{f}\right)^2 m_3'^2}\cos\alpha. \tag{11}$$

Dividing this by $m_3 m_3'$ and squaring this on both sides, we obtain

$$\left(\frac{\hat{f}}{f}\right)^4 \sin^2\alpha + \left(\frac{\hat{f}}{f}\right)^2 \left(2\left(\frac{m_1 m_1' + m_2 m_2'}{m_3 m_3'}\right) - \left(\frac{m_1^2 + m_2^2}{m_3^2} + \frac{m_1'^2 + m_2'^2}{m_3'^2}\right)\cos^2\alpha\right) + \left(\frac{m_1 m_1' + m_2 m_2'}{m_3 m_3'}\right)^2 - \frac{m_1^2 + m_2^2}{m_3^2}\cdot\frac{m_1'^2 + m_2'^2}{m_3'^2}\cos^2\alpha = 0. \tag{12}$$

This equation gives two values for $(\hat{f}/f)^2$; the one for which both sides of (11) have the same sign is chosen.

6. RELIABILITY OF FOCAL LENGTH

If the N-vectors $\boldsymbol{m}$ and $\boldsymbol{m}'$ are computed from a real image, they may contain errors. Suppose the tentative focal length f coincides with the exact value. Letting $\boldsymbol{m} \to \boldsymbol{m} + \Delta\boldsymbol{m}, \boldsymbol{m}' \to \boldsymbol{m}' + \Delta\boldsymbol{m}'$, and $\hat{f} \to f + \Delta f$ in (11), we obtain to a first approximation

$$\Delta f = -\frac{f((\Delta\boldsymbol{m}, \boldsymbol{m}') + (\boldsymbol{m}, \Delta\boldsymbol{m}'))}{2m_3m_3' - (m_3^2 + m_3'^2)\cos\alpha}, \tag{13}$$

where we have used the relationships $\|\boldsymbol{m}\| = 1$, $\|\boldsymbol{m}'\| = 1$, $(\boldsymbol{m}, \Delta\boldsymbol{m}) = 0$ and $(\boldsymbol{m}', \Delta\boldsymbol{m}') = 0$. If errors in $\boldsymbol{m}$ and $\boldsymbol{m}'$ are independent, its variance $V[f] = E[(\Delta f)^2]$ is given by

$$\begin{aligned} V[f] &= \frac{f^2(\boldsymbol{m}'^{\top} E[\Delta\boldsymbol{m}\Delta\boldsymbol{m}^{\top}]\boldsymbol{m}' + \boldsymbol{m}^{\top} E[\Delta\boldsymbol{m}'\Delta\boldsymbol{m}'^{\top}]\boldsymbol{m})}{(2m_3m_3' - (m_3^2 + m_3'^2)\cos\alpha)^2} \\ &= \frac{f^2((\boldsymbol{m}', V[\boldsymbol{m}]\boldsymbol{m}') + (\boldsymbol{m}, V[\boldsymbol{m}']\boldsymbol{m}))}{(2m_3m_3' - (m_3^2 + m_3'^2)\cos\alpha)^2}, \end{aligned} \tag{14}$$

where $V[\boldsymbol{m}]$ and $V[\boldsymbol{m}']$ are the covariance matrices of N-vectors $\boldsymbol{m}$ and $\boldsymbol{m}'$, respectively.

Suppose the two vanishing points are detected as intersections of N and N' concurrent image lines fitted to edge segments. Substitution of (9) into (14) yields the approximation

$$\begin{aligned} V[f] \approx \frac{6\kappa f^2}{(2m_3m_3' - (m_3^2 + m_3'^2)\cos\alpha)^2} \Bigg(&\frac{(\boldsymbol{m}_C, \boldsymbol{m}')^2}{\sum_{\alpha=1}^{N} w_\alpha^3 \sin^2\phi_\alpha / \sin^2\theta_\alpha} \\ &+ \frac{(\boldsymbol{m}_C', \boldsymbol{m})^2}{\sum_{\alpha=1}^{N'} w_\alpha'^3 \sin^2\phi_\alpha' / \sin^2\theta_\alpha'} \Bigg), \end{aligned} \tag{15}$$

where $\boldsymbol{m}_C$ and $\boldsymbol{m}_C'$ are the N-vectors of the points 'conjugate' [13] to the vanishing points on the 'center lines' of the two sets of image lines (Fig. 4b); w_α and w_α' are the lengths of the edge segments; ϕ_α and ϕ_α' are their 'deviation angles'; θ_α and θ_α' are the 'disparities' of the vanishing points from the center points of the individual edge segments.

Let θ and θ' be the disparities of the two vanishing points from the image origin o. We have the following relationship:

$$\begin{aligned} &(2m_3m_3' - (m_3^2 + m_3'^2)\cos\alpha)^2 \\ &\quad = (2\cos\theta\cos\theta' - (\cos^2\theta + \cos^2\theta')\cos\alpha)^2. \end{aligned} \tag{16}$$

Suppose the center lines of the two sets of image lines meet at the image origin o. Then,

PROPOSITION 1.

$$(\boldsymbol{m}_C, \boldsymbol{m}') = \frac{\cos\theta' - \cos\theta\cos\alpha}{\sin\theta},$$
$$(\boldsymbol{m}'_C, \boldsymbol{m}) = \frac{\cos\theta - \cos\theta'\cos\alpha}{\sin\theta'}. \tag{17}$$

Proof. In spherical coordinates, vectors $\boldsymbol{m}$ and $\boldsymbol{m}'$ have components

$$\boldsymbol{m} = \begin{pmatrix} \sin\theta\cos\phi \\ \sin\theta\sin\phi \\ \cos\theta \end{pmatrix}, \qquad \boldsymbol{m}' = \begin{pmatrix} \sin\theta'\cos\phi' \\ \sin\theta'\sin\phi' \\ \cos\theta' \end{pmatrix}. \tag{18}$$

Since $\boldsymbol{m}$ and $\boldsymbol{m}'$ make angle α, we have

$$\begin{aligned}(\boldsymbol{m}, \boldsymbol{m}') &= \sin\theta\sin\theta'(\cos\phi\cos\phi' + \sin\phi\sin\phi') + \cos\theta\cos\theta' \\ &= \sin\theta\sin\theta'\cos(\phi - \phi') + \cos\theta\cos\theta' = \cos\alpha,\end{aligned} \tag{19}$$

or

$$\cos(\phi - \phi') = \frac{\cos\alpha - \cos\theta\cos\theta'}{\sin\theta\sin\theta'}. \tag{20}$$

The N-vectors $\boldsymbol{m}_C$ and $\boldsymbol{m}'_C$ are expressed in spherical coordinates in the form

$$\boldsymbol{m}_C = \begin{pmatrix} -\cos\theta\cos\phi \\ -\cos\theta\sin\phi \\ \sin\theta \end{pmatrix}, \qquad \boldsymbol{m}'_C = \begin{pmatrix} -\cos\theta'\cos\phi' \\ -\cos\theta'\sin\phi' \\ \sin\theta' \end{pmatrix}. \tag{21}$$

Hence,

$$\begin{aligned}(\boldsymbol{m}, \boldsymbol{m}'_C) &= -\sin\theta\cos\theta'(\cos\phi\cos\phi' + \sin\phi\sin\phi') + \cos\theta\sin\theta' \\ &= -\sin\theta\cos\theta'\cos(\phi - \phi') + \cos\theta\sin\theta' \\ &= \frac{\cos\theta - \cos\theta'\cos\alpha}{\sin\theta'}.\end{aligned} \tag{22}$$

The first of (17) is obtained similarly. □

If the center points of the edge segments are close to the image origin o as compared with f, the disparities θ_α and θ'_α are all approximated by θ and θ', respectively.

Substituting (17) and (16) into (15), we obtain

$$V[f] \approx \frac{6\kappa f^2}{\left(2\cos\theta\cos\theta' - (\cos^2\theta + \cos^2\theta')\cos\alpha\right)^2} \times \left(\frac{\left(\cos\theta' - \cos\theta\cos\alpha\right)^2}{\sum_{\alpha=1}^{N} w_\alpha^3 \sin^2\phi_\alpha} + \frac{\left(\cos\theta - \cos\theta'\cos\alpha\right)^2}{\sum_{\alpha=1}^{N'} w_\alpha'^3 \sin^2\phi_\alpha'} \right). \tag{23}$$

7. OPTIMAL GRID CONFIGURATION

Consider a grid pattern placed in the scene (Fig. 6). Let r be the distance from the viewpoint O to the center of the grid pattern. Suppose the pattern consists of two sets of N (= an odd number) lines. Let l be the size of the pattern, and d the size of the individual grid line segments. If l/r is small, we have the following approximations:

$$w_\alpha \approx f\frac{l}{r}\sin\theta, \qquad w_\alpha' \approx f\frac{l}{r}\sin\theta'. \tag{24}$$

Let ϕ_0 and ϕ_0' be the deviation angles between neighboring grid lines in the two directions, respectively. If Nd/r is small, we have the approximations

$$\sum_{\alpha=1}^{N} \sin^2\phi_\alpha \approx 2\sum_{k=1}^{(N-1)/2} k^2\sin^2\phi_0 = \frac{N(N^2-1)}{12}\sin^2\phi_0,$$

$$\sum_{\alpha=1}^{N} \sin^2\phi_\alpha' \approx 2\sum_{k=1}^{(N-1)/2} k^2\sin^2\phi_0' = \frac{N(N^2-1)}{12}\sin^2\phi_0'. \tag{25}$$

Let $\boldsymbol{k} = (0, 0, 1)^\top$. We assume that $\boldsymbol{m}$ and $\boldsymbol{m}'$ are oriented so that $|\boldsymbol{m}, \boldsymbol{m}', \boldsymbol{k}| > 0$.

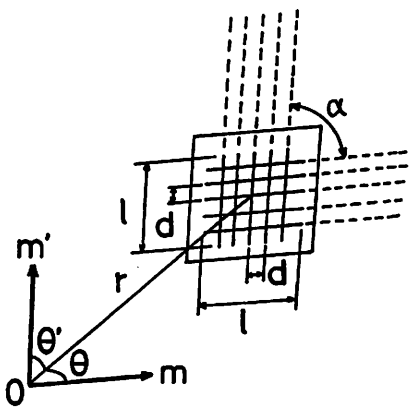

Figure 6. The 3D configuration of the grid pattern.

PROPOSITION 2.

$$\sin\phi_0 = \frac{d}{r}\frac{|m, m', k|}{\sin^2\theta} + O\left(\left(\frac{d}{r}\right)^2\right),$$
$$\sin\phi_0' = \frac{d}{r}\frac{|m, m', k|}{\sin^2\theta'} + O\left(\left(\frac{d}{r}\right)^2\right). \tag{26}$$

Proof. The N-vector of the central grid line that extends in the direction of m is

$$n_0 = N[m \times k] = \frac{m \times k}{\|m \times k\|} = \frac{m \times k}{\sin\theta}. \tag{27}$$

If $d/r \ll 1$, the N-vector of the neighboring grid line is

$$n_1 = N[m \times (rk + dm')] = c\left(m \times k + \frac{d}{r} m \times m'\right), \tag{28}$$

where

$$c = \frac{1}{\|m \times k + (d/r)m \times m'\|} = \frac{1}{\|m \times k\|} + O\left(\frac{d}{r}\right)$$
$$= \frac{1}{\sin\theta} + O\left(\frac{d}{r}\right). \tag{29}$$

From the definition of the deviation angle ϕ_0, we have $\sin\phi_0 = \|n_0 \times n_1\|$. Equations (27) and (28) imply

$$n_1 \times n_0 = \frac{cd}{r}\frac{(m \times m') \times (m \times k)}{\sin\theta} = \frac{cd}{r}\frac{|m, m', k|m}{\sin\theta}. \tag{30}$$

From (29), we obtain the first of (26). The second equation is obtained similarly. □

Substituting (26) into (25) and substituting the result into (15) together with (24), we obtain

$$V[f]$$
$$\approx \frac{72\kappa r^5\left(\sin\theta\left(\cos\theta' - \cos\theta\cos\alpha\right)^2 + \sin\theta'\left(\cos\theta - \cos\theta'\cos\alpha\right)^2\right)}{N(N^2-1)fd^2l^3\left(2\cos\theta\cos\theta' - \left(\cos^2\theta + \cos^2\theta'\right)\cos\alpha\right)^2|m, m', k|^2}. \tag{31}$$

PROPOSITION 3.

$$|\boldsymbol{m}, \boldsymbol{m}', \boldsymbol{k}|^2 = \frac{1}{\sin^2\alpha}\Big(\sin^4\alpha - \big(\cos\theta - \cos\theta'\cos\alpha\big)^2 - \big(\cos\theta' - \cos\theta\cos\alpha\big)^2 - 2\big(\cos\theta - \cos\theta'\cos\alpha\big)\big(\cos\theta' - \cos\theta\cos\alpha\big)\cos\alpha\Big). \quad (32)$$

Proof. Three vectors $\boldsymbol{m}$, $\boldsymbol{m}'$ and $\boldsymbol{m} \times \boldsymbol{m}'$ are linearly independent. Hence, vector $\boldsymbol{k}$ can be expressed in the form

$$\boldsymbol{k} = A\boldsymbol{m} + B\boldsymbol{m}' + c\boldsymbol{m} \times \boldsymbol{m}'. \quad (33)$$

Since vector $\boldsymbol{m}$ makes angle θ with $\boldsymbol{k}$, we have $(\boldsymbol{m}, \boldsymbol{k}) = \cos\theta$. Using $(\boldsymbol{m}, \boldsymbol{m}) = 1$, $(\boldsymbol{m}, \boldsymbol{m}') = \cos\alpha$ and $(\boldsymbol{m}, \boldsymbol{m} \times \boldsymbol{m}') = 0$, we obtain

$$A + B\cos\alpha = \cos\theta. \quad (34)$$

Similarly, we obtain from $(\boldsymbol{m}', \boldsymbol{k}) = \cos\theta'$

$$A\cos\alpha + B = \cos\theta'. \quad (35)$$

From these two equations, we obtain

$$A = \frac{\cos\theta - \cos\theta'\cos\alpha}{\sin^2\alpha}, \qquad B = \frac{\cos\theta' - \cos\theta\cos\alpha}{\sin^2\alpha}. \quad (36)$$

Since $\boldsymbol{k}$ is a unit vector, we have

$$\begin{aligned}\|\boldsymbol{k}\|^2 &= A^2\|\boldsymbol{m}\|^2 + B^2\|\boldsymbol{m}'\|^2 + C^2\|\boldsymbol{m} \times \boldsymbol{m}'\|^2 \\ &\quad + 2AB(\boldsymbol{m}, \boldsymbol{m}') + 2AC(\boldsymbol{m}, \boldsymbol{m} \times \boldsymbol{m}') + 2BC(\boldsymbol{m}', \boldsymbol{m} \times \boldsymbol{m}') \\ &= A^2 + B^2 + C^2\sin^2\alpha + 2AB\cos\alpha = 1. \end{aligned} \quad (37)$$

Hence,

$$C^2 = \frac{1 - A^2 - B^2 - 2AB\cos\alpha}{\sin^2\alpha}. \quad (38)$$

Noting that

$$|\boldsymbol{m}, \boldsymbol{m}', \boldsymbol{k}| = (\boldsymbol{m} \times \boldsymbol{m}', \boldsymbol{k}) = C\|\boldsymbol{m} \times \boldsymbol{m}'\|^2 = C\sin^2\alpha, \quad (39)$$

we obtain (32). □

The angles θ and θ' that minimize $V[f]$ for a given α are given as follows:

THEOREM 1. *The variance $V[f]$ is minimized when*

$$\theta = \theta' = \sin^{-1}\sqrt{\frac{1+\sin^2(\alpha/2)+\sqrt{\sin^4(\alpha/2)+14\sin^2(\alpha/2)+1}}{6}}, \tag{40}$$

for which the projections of the grid lines meet at angle

$$\gamma = \pi - \cos^{-1}\frac{2\sin^2(\alpha/2)-\sin^2\theta}{\sin^2\theta}. \tag{41}$$

Proof. It is easy to confirm that the left-hand side of (31) takes its minimum when $\theta = \theta'$. Letting $\theta = \theta'$ in (31), we obtain

$$V[f] \approx \frac{36\kappa r^5 \sin\theta}{N(N^2-1)fd^2l^3|\boldsymbol{m},\boldsymbol{m}',\boldsymbol{k}|^2}. \tag{42}$$

From (32), we obtain

$$|\boldsymbol{m},\boldsymbol{m}',\boldsymbol{k}|^2 = \frac{\sin^4\alpha - 2\cos^2\theta(1-\cos\alpha)^2(1+\cos\alpha)}{\sin^2\alpha}. \tag{43}$$

If we note that $\sin\alpha = 2\sin(\alpha/2)\cos(\alpha/2)$, $1+\cos\alpha = 2\cos^2(\alpha/2)$ and $1-\cos\alpha = 2\sin^2(\alpha/2)$, (43) is rewritten in the following form:

$$|\boldsymbol{m},\boldsymbol{m}',\boldsymbol{k}| = 4\sin^2\frac{\alpha}{2}\left(\cos^2\frac{\alpha}{2}-\cos^2\theta\right). \tag{44}$$

Hence

$$V[f] \approx \frac{9\kappa r^5}{N(N^2-1)fd^2l^3}\frac{\sin\theta}{\sin^2(\alpha/2)\cos^2\theta\left(\cos^2(\alpha/2)-\cos^2\theta\right)}. \tag{45}$$

Since $\cos^2\theta = 1-\sin^2\theta$ and $\cos^2(\alpha/2)-\cos^2\theta = \sin^2\theta-\sin^2\alpha/2$, the right-hand side is written as

$$\frac{9\kappa r^5}{N(N^2-1)fd^2l^3}F\left(\sin^2\frac{\alpha}{2},\sin\theta\right), \tag{46}$$

where

$$F(a,x) = \frac{x}{a(1-x^2)(x^2-a)}. \tag{47}$$

Differentiating this function with respect to x, we see that for $\sqrt{a} < x < 1$ it is minimized when

$$x = \sqrt{\frac{1+a+\sqrt{a^2+14a+1}}{6}}. \tag{48}$$

Hence, the optimal values θ and θ' are given by (40). For these angles, (20) implies that the angle γ made by the two sets of grid lines is given by

$$\cos\gamma = -\frac{\cos^2\theta - \cos\alpha}{\sin^2\theta} = -\frac{2\sin^2(\alpha/2) - \sin^2\theta}{\sin^2\theta}, \tag{49}$$

from which (41) is obtained. □

COROLLARY 1. *In the optimal configuration, the grid pattern makes angle*

$$\beta = \cos^{-1}\sqrt{\frac{1 - 5\sin^2(\alpha/2) + \sqrt{\sin^4(\alpha/2) + 14\sin^2(\alpha/2) + 1}}{6\cos^2(\alpha/2)}} \tag{50}$$

from the image plane.

Proof. The unit surface normal to the grid pattern is

$$\boldsymbol{n} = N[\boldsymbol{m} \times \boldsymbol{m}'] = \frac{\boldsymbol{m} \times \boldsymbol{m}'}{\sin\alpha}. \tag{51}$$

If β is the angle between $\boldsymbol{n}$ and $\boldsymbol{k}$, we obtain

$$\cos\beta = (\boldsymbol{n}, \boldsymbol{k}) = \frac{|\boldsymbol{m}, \boldsymbol{m}', \boldsymbol{k}|}{\sin\alpha}. \tag{52}$$

Using (44), we see that

$$\cos^2\beta = \frac{\sin^2\theta - \sin^2(\alpha/2)}{\cos^2(\alpha/2)}. \tag{53}$$

Substituting (40), we obtain (50). □

In intuitive terms, the pattern needs to be inclined to make a large angle from the image plane so that the effect of foreshortening is strong. However, too much inclination compresses the resulting image of the grid pattern, decreasing the lengths of the edge segments and the separations between them, thereby decreasing the accuracy of the detected vanishing points. The optimal balance is attained at the values of (40), (41) and (50).

8. OPTIMAL GRID SHAPE

We now optimize the angle α.

THEOREM 2. *The angle α that minimizes $V[f]$ in the optimal configuration of the pattern is*

$$\alpha = 2\sin^{-1}\sqrt{\frac{3}{10}} = 66.42182152\ldots^\circ. \tag{54}$$

The corresponding optimal configuration is given by

$$\theta = \theta' = \sin^{-1}\sqrt{\frac{3}{5}} = 50.76847951\ldots^\circ. \tag{55}$$

If the pattern is in the optimal configuration, the two grid lines meet orthogonally on the image plane.

Proof. All we need to do is minimize (47) with respect to α. We have

$$\frac{dF}{da} = \frac{\partial F}{\partial a} + \frac{\partial F}{\partial x}\frac{dx}{da} = \frac{\partial F}{\partial a}, \tag{56}$$

because $\partial F/\partial x = 0$ for the optimal value of x. Since

$$\frac{\partial F}{\partial a} = \frac{x}{1-x^2}\frac{2a-x^2}{a^2(x^2-a)^2}, \tag{57}$$

we obtain $a = x^2/2$. Hence, (48) implies

$$a = \frac{1+a+\sqrt{a^2+14a+1}}{12}, \tag{58}$$

from which we obtain $a = 3/10$. By definition $a = \sin^2(\alpha/2)$, so we obtain (54). From $a = x^2/2$, we have $x = \sqrt{(2a)}$. By definition $x = \sin\theta$, so we obtain $\sin\theta = \sqrt{3/5}$ and hence (55). For these values of α and θ, (49) implies $\cos\gamma = 0$ or $\gamma = \pi/2$. □

COROLLARY 2. *In the optimal configuration, the optimal grid pattern makes angle*

$$\beta = \cos^{-1}\sqrt{\frac{3}{7}} = 49.1066053\ldots^\circ \tag{59}$$

from the image plane.

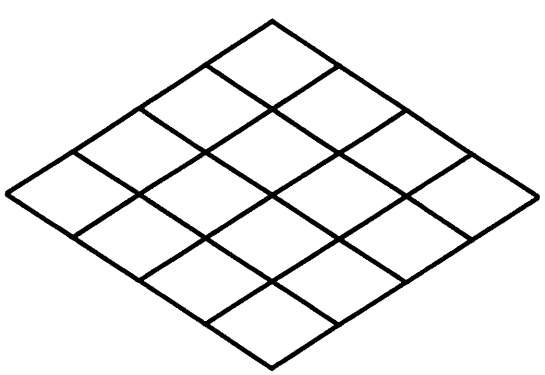

Figure 7. Optimal grid pattern.

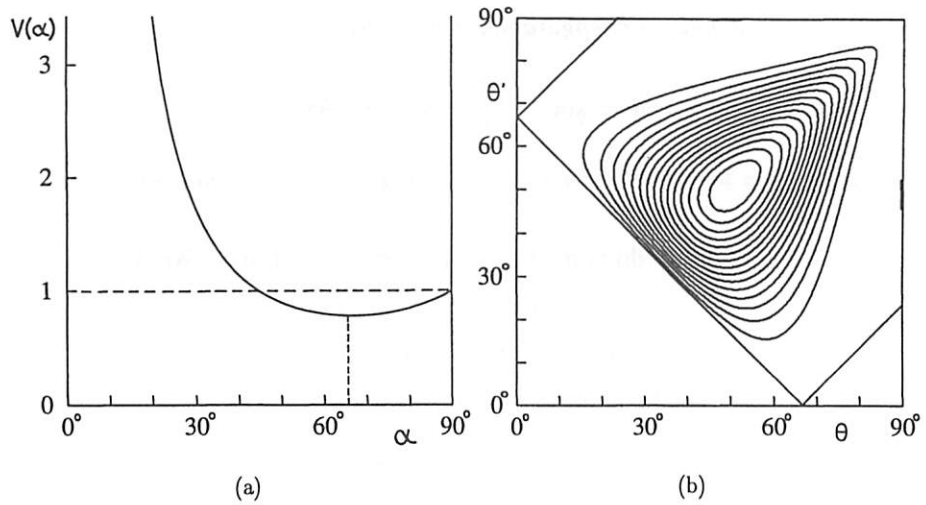

Figure 8. (a) The graph of $V(\alpha)$ in the scale for which $V(\pi/2) = 1$. (b) The contours of $1/V(\theta, \theta', \alpha)$ for the optimal value of α.

Figure 7 shows the optimal grid pattern for $N = 5$. Put the right-hand side of (31) to be $V(\theta, \theta', \alpha)$ and let $V(\alpha) = \min_{\theta,\theta'} V(\theta, \theta', \alpha)$. Figure 8(a) shows the graph of $V(\alpha)$ for $0 < \alpha \leqslant \pi$, where we use the scale for which $V(\pi/2) = 1$. Its minimum is $0.78196029\ldots$. This means that the error in f computed from the optimal grid pattern is about 88% of the error for the square grid pattern. Figure 8(b) shows the contours of the graph of $1/V(\theta, \theta', \alpha)$ for the optimal value α. The domain of $V(\theta, \theta', \alpha)$ is $|\theta + \theta'| < \alpha$ and $|\theta - \theta'| < \alpha$.

9. DESIGN OF THE PATTERN

Although the theoretical analysis based on an idealized mathematical model has been completed, many realistic considerations are necessary in actually designing the pattern for practical use.

9.1. Orientation of the tilt

Theoretically, the pattern can be inclined in any orientation; the tilt orientation is arbitrary. In real environments, light sources are usually fixed on the ceiling, so it is the most convenient to choose the tilt orientation to be horizontal and keep the camera optical axis (approximately) horizontal. If the pattern is drawn on a semi-transparent plate, a light source can be placed right under it.

9.2. Shape of the grid region

Suppose the tilt is horizontal and the camera is located so that the entire pattern appears in the image. If the grid is drawn in a rectangular region and the image frame is square, the background appears near the upper right and upper left corners due to

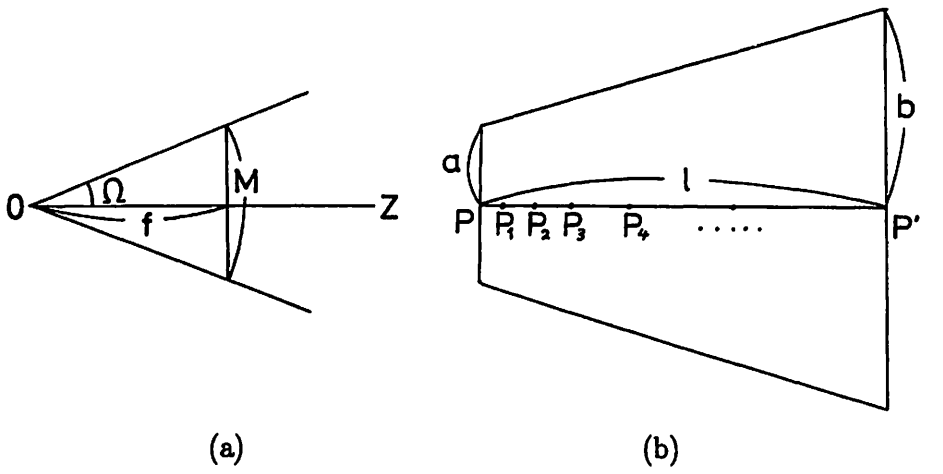

Figure 9. (a) The half angle of view Ω. (b) The optimal trapezoidal region.

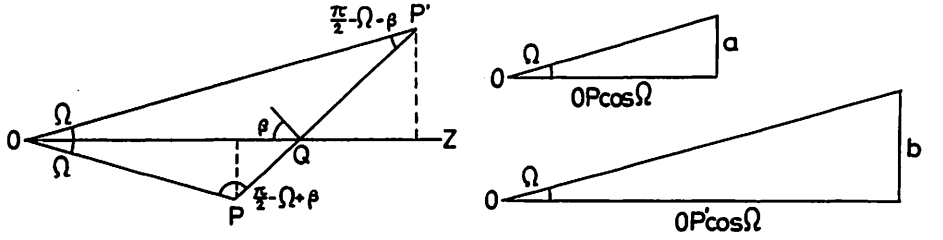

Figure 10. The geometry of the pattern placed in the scene.

foreshortening. This is avoided by drawing the grid in an 'upside-down trapezoid' region so that its projection becomes a square.

Let Ω be the half angle of view: if the image frame has $M \times M$ pixels and the focal length is f pixels (Fig. 9a), we have $\Omega = \tan^{-1}(M/2)$. Consider the trapezoidal region shown in Fig. 9(b). Figure 10(a) shows the geometry in the scene when this trapezoid is slanted by angle β. Applying the sine rule to triangles ΔOPQ and $\Delta OP'Q$, we obtain

$$PQ = \frac{\sin \Omega}{\cos(\Omega - \beta)}, \qquad OP = \frac{\cos \beta}{\cos(\Omega - \beta)} OQ, \tag{60}$$

$$P'Q = \frac{\sin \Omega}{\cos(\Omega + \beta)}, \qquad OP' = \frac{\cos \beta}{\cos(\Omega + \beta)} OQ. \tag{61}$$

From Fig. 10(b), we see that

$$a = \frac{\sin \Omega \cos \beta}{\cos(\Omega - \beta)}, \qquad b = \frac{\sin \Omega \cos \beta}{\cos(\Omega + \beta)}. \tag{62}$$

The height of the trapezoid is $l = PQ + PQ'$, so

$$l = \sin\Omega\left(\frac{1}{\cos(\Omega+\beta)} + \frac{1}{\cos(\Omega-\beta)}\right)OQ. \tag{63}$$

Thus, the shape of the trapezoid is determined by the ratio

$$a : b : l = \cos\beta\cos(\Omega+\beta) : \cos\beta\cos(\Omega-\beta) : \cos(\Omega+\beta) + \cos(\Omega-\beta). \tag{64}$$

This shape depends on the angle Ω, which depends on the focal length f to be calibrated. In real environments, it is easy to estimate an approximate value of the focal length for a real camera. Otherwise, we can prepare several fixed prototype patterns, say for wide-angle lenses, standard lenses and telephoto lenses.

9.3. Thickness of the grid lines

If the grid lines do not have sufficient thickness, their projections become very thin in the upper region due to foreshortening, so accurate detection of the grid lines in the image becomes difficult. However, if the grid lines are drawn very thick, their projections become too thick in the lower region, reducing the accuracy of line fitting.

This problem can be resolved by varying the thickness so that the projected lines have constant thickness. Namely, the thickness is made proportional to the distance from the camera. If the distance variation along the tilt orientation is ignored, we see from Fig. 10(a) that the ratio of the thickness at the nearest end to that at the remotest and should be OP: OP'. From (60) and (61), this ratio equals $\cos(\Omega+\beta)$: $\cos(\Omega-\beta)$.

9.4. Separation between grid lines

The accuracy of calibration increases as the number of grid lines increases. However, if the number of grid lines is extremely large, the projected grid becomes too dense in the upper region, causing difficulties in edge detection and line fitting. This problem can be resolved by preparing a grid of varying coarseness in such a way that its projection has an approximately uniform coarseness over the image.

Consider the intersections $(P =)P_0, P_1, \ldots, P_N\ (= P')$ of the center line PP' with the grid lines in Fig. 9(b). If points $\{P_k\}$ are to be projected in equidistance on the image plane, they should be chosen so that

$$PP_k = \frac{l\cos(\Omega+\beta)}{\cos(\Omega+\beta)+\cos(\Omega-\beta)}\left(1 - \frac{\sin(\Omega-2\Omega k/N)\cos(\Omega-\beta)}{\sin\Omega\cos(\Omega-\beta-2\Omega k/N)}\right). \tag{65}$$

9.5. Estimating the image accuracy

In order to evaluate the confidence interval of the computed focal length f, we need to evaluate the variance $V[f]$ given by (14), which requires the values of the covariance matrices $V[\boldsymbol{m}']$ and $V[\boldsymbol{m}]$ given in the form of (8). Hence, we must compute the moment matrix $\boldsymbol{N}$ given by (7) and consequently the optimal weights W_α given by (5).

Thus, we need to compute the covariance matrix $V[\boldsymbol{n}_\alpha]$ given by (2) for each edge segment, but this requires the value of the image resolution κ defined by (3).

A safe estimate of the image accuracy ε, which describes the perturbation of each edge pixel, is the 'average half-width' of the lines in the image. In the binary image obtained by thresholding, we compute the 'total area' (i.e. the number of pixels) of the lines in it. After thinning them, we compute their 'total length' and regard the total area divided by the total length as the 'average width'. The edge density ρ is estimated by dividing the number of total edge pixels by the total length.

9.6. Final design

Figure 11 shows the pattern designed with these considerations. Figure 12(a) is a real image of this pattern, and Fig. 12(b) shows fitted lines. The focal length is estimated to be $f = 694.38$ (pixels). The average width of the lines is 7.22 pixels, so $\varepsilon \approx 3.62$ (pixels). The edge density is $\rho \approx 0.81$ (1/pixels). Hence, the image resolution is $\kappa = 16.21$. The standard deviation of f is estimated to be $\sqrt{V[f]} = 0.91$ (pixels). This means that the 95% confidence interval is [693.47, 695.27]. If the positions of the pattern and the camera are slightly disturbed, the computed estimate of f fluctuates slightly, but it has been experimentally confirmed that the fluctuations are roughly within the computed confidence interval.

In doing the above experiment, we placed the optimal grid pattern on a transparent box with an optimally inclined top face (Fig. 13a). A light source was installed inside the box. If this box is placed so that its front face is (approximately) parallel to the image plane and the camera is placed so that its optical axis is (approximately) horizontal, the calibration attains (approximately) the theoretically optimal performance. We used a grid pattern consisting of lines, but a checker board pattern can also be used (Fig. 13b). In this case, the necessary image processing stages are different. Each pattern has its advantages and disadvantages, and it is difficult to decide which is advantageous over the other.

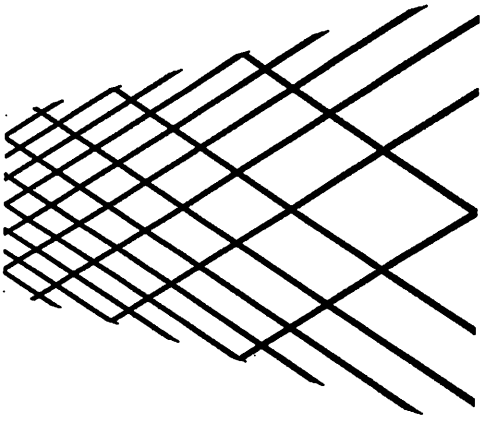

Figure 11. The optimal grid with varying thickness and varying separations.

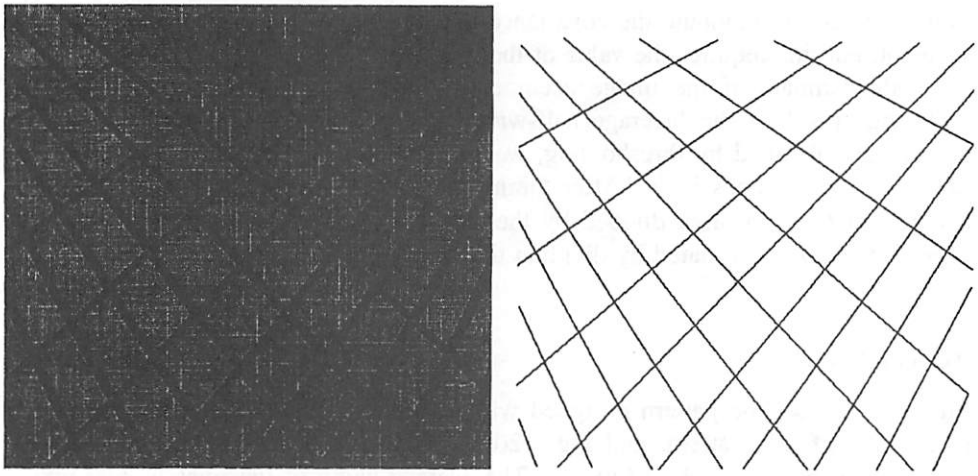

(a) (b)

Figure 12. (a) A real image of the pattern of Fig. 11. (b) Fitted lines.

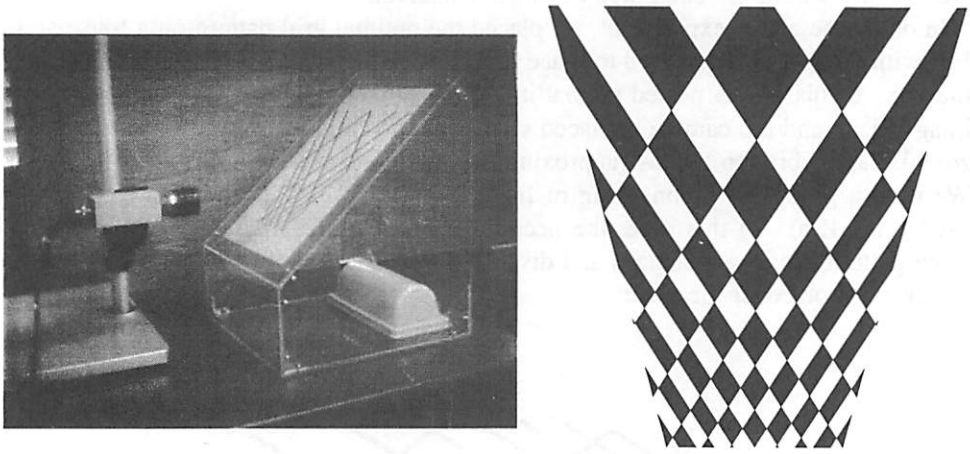

(a) (b)

Figure 13. (a) The optimal grid pattern is optimally fixed. (b) The optimal checkerboard pattern.

In our experiment, we ignored lens aberration and assumed that the aspect ratio was 1. We also assumed that the image origin was at the frame center. In order to improve the accuracy of the focal length further, these factors should also be calibrated accurately, but we do not go into the detail here.

10. CONCLUDING REMARKS

We have obtained a theoretically optimal grid pattern for focal length calibration that maximizes the reliability of the computed value. Although the improvement is not very large as compared with the use of a square grid pattern, this is a good example of the fact that maximum reliability can be attained by carefully analyzing the geometry of the problem and the statistical behavior of noise. The computation involved is essentially the same for any grid pattern, so there is no reason to use a square grid pattern, which has been favored by many people in the past. We have designed a convenient device after incorporating realistic considerations – the orientation of the tilt, the shape of the grid region, the thickness of the grid lines and the separation between grid lines. Our device is expected to be used widely as a standard tool in robotics research.

Acknowledgments

This work was in part supported by the Ministry of Education, Science, Sports, and Culture, Japan and under a Grant in Aid for Scientific B (no. 07458067) and the Okawa Institute of Information and Telecommunication.

REFERENCES

1. B. Caprile and V. Torre, "Using vanishing points for camera calibration," *Int. J. Comput. Vision*, vol. 4, pp. 127–140, 1990.
2. T. Echigo, "A camera calibration technique using three sets of parallel lines," *Machine Vision Appl.*, vol. 3, pp. 159–167, 1990.
3. W. I. Grosky and L. A. Tamburino, "A unified approach to the linear camera calibration problem," *IEEE Trans. Pattern Anal. Machine Intell.*, vol. 12, pp. 663–671, 1990.
4. K. Kanatani and Y. Onodera, "Anatomy of camera calibration using vanishing points," *IEICE Trans. Inf. Syst.*, vol. E74-D, no. 10, pp. 3369–3378, 1991.
5. J. Z. C. Lai, "On the sensitivity of camera calibration," *Image Vision Comput.*, vol. 11, no. 10, pp. 656–664, 1993.
6. R. K. Lenz and R. Y. Tsai, "Techniques for calibration of the scale factor and image center for high-accuracy 3D machine vision metrology," *IEEE Trans. Pattern Anal. Machine Intell.*, vol. 10, pp. 713–720, 1988.
7. R. K. Lenz and R. Y. Tsai, "Calibrating a Cartesian robot with eye-on-hand configuration independent of eye-to-hand relationship," *IEEE Trans. Pattern Anal. Machine Intell.*, vol. 11, pp. 916–928, 1989.
8. M. A. Penna, "Camera calibration: A quick and easy way to determine the scale factor," *IEEE Trans. Pattern Anal. Machine Intell.*, vol. 13, pp. 1240–1245, 1991.
9. R. Y. Tsai and R. K. Lenz, "A new technique for fully autonomous and efficient 3D robotics hand/eye calibration," *IEEE Trans. Robotics Automat.*, vol. 5, pp. 345–358, 1989.
10. L.-L. Wang and W.-H. Tsai, "Camera calibration by vanishing lines for 3-D computer vision," *IEEE Trans. Pattern Anal. Machine Intell.*, vol. 13, pp. 370–376, 1991.
11. K. Kanatani, "Statistical analysis of focal length calibration using vanishing points," *IEEE Trans. Robotics Automat.*, vol. 8, pp. 767–775, 1992.
12. K. Kanatani, *Group-Theoretical Methods in Image Understanding*. Berlin: Springer, 1990.
13. K. Kanatani, "Computational projective geometry," *CVGIP: Image Understanding*, vol. 54, pp. 333–348, 1991.
14. K. Kanatani, *Geometric Computation for Machine Vision*. Oxford: Oxford University Press, 1993.
15. K. Kanatani, "Statistical analysis of geometric computation," *CVGIP: Image Understanding*, vol. 59, pp. 286–306, 1994.

APPENDIX: SUMMARY OF COMPUTATION

The procedure for computing the focal length and its confidence interval is summarized as follows:

(1) Take an image of a grid pattern, detect grid lines by thresholding and thinning, and compute the length of each edge segment, the average width, and the edge density. Then, fit lines to them by least squares. Let $\{l_\alpha\}$, $\alpha = 1, \ldots, N$, and $\{l'_\alpha\}$, $\alpha = 1, \ldots, N'$ be the two sets of the fitted lines in the two directions, where N and N' are the numbers of the detected lines in the two directions. Let the image resolution be $\kappa = d^2/4\rho$, where d is the average width of the lines and ρ is the edge density.

(2) Assuming a tentative focal length f, compute the N-vectors $\boldsymbol{n}_\alpha$ and $\boldsymbol{n}'_\alpha$ of the lines l_α and l'_α, $\alpha = 1, \ldots, N$.

(3) Compute the covariance matrices $V[\boldsymbol{n}_\alpha]$ and $V[\boldsymbol{n}'_\alpha]$ of N-vectors $\boldsymbol{n}_\alpha$ and $\boldsymbol{n}'_\alpha$, $\alpha = 1, \ldots, N$, by (2).

(4) Compute the N-vector $\boldsymbol{m}$ of the vanishing point of lines $\{l_\alpha\}$ and its covariance matrix $V[\boldsymbol{m}]$ by the following procedure called *renormalization* [7]:

(4.1) Let $c = 0$ and $W_\alpha = 1$, $\alpha = 1, \ldots, N$.

(4.2) Compute the unit eigenvector $\boldsymbol{m}$ of the *unbiased moment matrix*

$$\widehat{N} = \sum_{\alpha=1}^{N} W_\alpha \left(\boldsymbol{n}_\alpha \boldsymbol{n}_\alpha^\top - cV[\boldsymbol{n}_\alpha]\right) \tag{A1}$$

for the smallest eigenvalue λ_m.

(4.3) Update c and W_α as follows:

$$c \leftarrow c + \frac{\lambda_m}{\sum_{\alpha=1}^{N} W_\alpha (\boldsymbol{m}, V[\boldsymbol{n}_\alpha]\boldsymbol{m})},$$

$$W_\alpha \leftarrow \frac{1}{(\boldsymbol{m}, V[\boldsymbol{n}_\alpha]\boldsymbol{m})}. \tag{A2}$$

(4.4) If the update has not converged, go back to Step (4.2). Otherwise, compute the largest and intermediate eigenvalues λ_u and λ_v of $\widehat{N}$ and the corresponding unit eigenvectors $\boldsymbol{u}$ and $\boldsymbol{v}$.

(4.5) Compute the covariance matrix $V[\boldsymbol{m}]$ by (8).

(4.6) Return the N-vector $\boldsymbol{m}$ and its covariance matrix $V[\boldsymbol{m}]$.

(5) Similarly, compute the N-vector $\boldsymbol{m}'$ of the vanishing point of lines $\{l'_\alpha\}$ and its covariance matrix $V[\boldsymbol{m}']$.

(6) Compute the true focal length $\hat{f}$ by solving (12) and compute its variance $V[f]$ by (14).

(7) The standard deviation is $\sqrt{V[\hat{f}]}$ and the $(100 - \alpha)\%$ confidence interval is

$$\left[\hat{f} - \lambda_a \sqrt{V[\hat{f}]}, \hat{f} + \lambda_a \sqrt{V[\hat{f}]}\right], \tag{A3}$$

where λ_a is the $a\%$ point of the standard normal distribution (i.e. $\lambda_5 = 1.96$).

ABOUT THE AUTHORS

Kenichi Kanatani received his PhD in Applied Mathematics from the University of Tokyo in 1979. He is currently Professor of Computer Science at Gunma University and studying mathematical methods for computer vision and robotics. He is the author of *Group-Theoretical Methods in Image Understanding* (Springer, 1990) and *Geometric Computation for Machine Vision* (Oxford University Press, 1993).

Tamotsu Maruyama received his MS in Computer Science from Gunma University in 1995. He is currently developing computer software at Altron Co.